Effect of conventionally neutral boundary layer height on turbine performance and wake mixing in offshore windfarms

Effect of conventionally neutral boundary layer height on turbine performance and wake mixing in offshore windfarms

Ishaan Sood[1], Wim Munters[2] and Johan Meyers[1]

[1]Department of Mechanical Engineering, KU Leuven, Celestijnenlaan 300A, 3001, Leuven, Belgium.
[2]Department of Mathematics and Computer Science, TU Eindhoven, Groeneloper 5, 5612 AZ Eindhoven, Netherlands.

E-mail: ishaan.sood@kuleuven.be, w.v.m.munters@tue.nl, johan.meyers@kuleuven.be

Abstract. In this study, we investigate the effect of conventionally neutral boundary layer height and capping inversion strength on wind farm performance. An aeroelastic multibody solver coupled with a pseudo-spectral large eddy simulation code is used to investigate the structural and aerodynamic output of wind turbines in 4 different inflow types. Farm layouts comprising of turbines in both aligned and staggered arrangements are studied. It is found that the shallower boundary layers with strong capping inversions are characterized by oscillatory structures in turbine wakes, leading to increased structural damage in downstream wind turbines due to fatigue. The power output is also observed to decrease due to poorer wake mixing.

1. Introduction

Recent years have seen the use of Large Eddy Simulations (LES) to model and study wind farms in the presence of classical Pressure Driven Boundary Layers (PDBL) [1, 2]. Allaerts and Meyers extended on this work by including Coriolis effects and thermal stability in the atmosphere, and simulating wind farms in a neutral boundary layer developing against a stably-stratified free atmosphere, called Conventionally Neutral Boundary Layers (CNBL) [3]. These boundary layers are significant due to the presence of an inversion layer with a strong temperature jump between the neutral boundary layer and the free atmosphere, and often occur in offshore conditions. The strength and height of this capping inversion affects the turbulence in the boundary layer below, influencing the energy available for extraction by wind farms. Additionally, with increase in offshore turbine size, the possibility of turbines operating near and within the capping inversion for shallow boundary layers is becoming a reality and hence the effect on turbine performance in these regimes is increasingly becoming important to understand.

In this work, we investigate the operation of wind farms in different neutral boundary layer heights. Aeroelastic wind turbine performance and wake mixing in the farm is analyzed to determine the effect of boundary layer height on performance. In section 2, the fluid and structural solver used in this research are detailed. Next, section 3 outlines the case setup and results are discussed in section 4. Finally, section 5 outlines the conclusions and future work.

2. Methodology

2.1. Fluid solver

Simulations are based on the spatially filtered three-dimensional Navier-Stokes momentum, continuity and temperature equations

$$\frac{\partial \tilde{u}}{\partial t} + (\tilde{u} \cdot \nabla)\tilde{u} = -\frac{\nabla(\tilde{p} + p_\infty)}{\rho} - \nabla \cdot \tau_s + 2\omega \times \tilde{u} + g\frac{(\tilde{\theta} - \theta_0)}{\theta_0} + \tau_w + f \tag{1}$$

$$\frac{\partial \tilde{\theta}}{\partial t} + (\tilde{u} \cdot \nabla)\tilde{\theta} = -\nabla \cdot q_s \tag{2}$$

which are solved using Large Eddy Simulations by means of SP-Wind, an in-house LES code developed at KU Leuven [4]. In these equations, $\tilde{u}$ and $\tilde{p}$ represent the filtered velocity and pressure fields respectively. The pressure gradient is split into a pressure gradient ∇p_∞ driving the mean flow and a fluctuating component $\nabla \tilde{p}$. High Reynolds numbers in atmospheric boundary-layer flows combined with typical spatial resolutions in LES justify the omission of resolved effects of viscous momentum transfer and diffusive heat transfer. These are represented by modeling the subgrid-scale stress tensor τ_s and the subgrid-scale heat flux q_s originating from spatially filtering the original governing equations. Coriolis effects are included through the Earth's angular velocity vector ω, and thermal buoyancy is represented by $g(\tilde{\theta} - \theta_0)/\theta_0$, with g the gravitational acceleration, $\tilde{\theta}$ the filtered potential temperature and θ_0 a reference temperature. The effect of the sea surface is included using a rough-wall stress model τ_w, that is based on the assumption of a logarithmic velocity profile with a roughness length z_0. f represents any remaining body forces on the flow.

Spatial discretization in the horizontal directions is performed by pseudo-spectral schemes and by fourth-order energy-conservative finite differences in the vertical direction. A fully explicit fourth-order Runge-Kutta scheme is used for time integration, and grid partitioning is achieved through a scalable pencil decomposition approach. Subgrid-scale stresses are modeled with a standard Smagorinsky model with wall damping. The subgrid-scale heat flux is calculated from the resolved potential temperature profile using an eddy-diffusivity model. Turbulent inflow conditions for wind-farm simulations are generated in separate concurrent precursor simulations and are introduced in the wind-farm domain by means of body forces in a so-called fringe region[5, 6].

2.2. Structural solver

Parametrization of the wind turbines on the LES grid is achieved by the use of an Aeroelastic Actuator Sector Model (AASM) [7]. This model is more accurate than the simpler Actuator Disc Model (ADM) while being computationally less expensive than the Actuator Line Model (ALM) due to a lower requirement of spatio-temporal resolution. In the AASM, the turbine blades sweep a sector area during each LES time step and the aerodynamic forces developed by the blade are added to the flow equations. A finite-element floating frame of reference (FFR) formulation is employed for solving the deformations in the turbine blades and tower multibody system due to the aerodynamic loads. Bryant angles are used to describe the orientation of the system. The rotation around the low speed shaft contributes to the dynamic behaviour of the system while yawing,tilting and preconing motions are taken into account quasistatically. The equation of motions for the rotor-tower system can be written as

$$\mathbf{M(q)\ddot{q} + C\dot{q} + K(q)q} + \boldsymbol{\phi}_{\boldsymbol{q}}^{\boldsymbol{T}}\boldsymbol{\lambda} = \boldsymbol{Q_a} + \boldsymbol{Q_g} + \boldsymbol{Q_v} \tag{3}$$

$$\boldsymbol{\phi(q)} = \mathbf{0} \tag{4}$$

where, $\mathbf{M}$, $\mathbf{C}$, $\mathbf{K}$, are the mass, damping and stiffness matrices respectively, computed using the structural specifications of the DTU 10MW wind turbine[8]. The vector $\mathbf{q}$ represents the

Table 1. Simulation parameters

Case	Boundary layer height	Inflow wind direction	Mean inflow velocity
PDk 90	1500 m	90°	9.4 m/s
CNk2 30	500 m	30°	11 m/s
CNk2 60	500 m	60°	11 m/s
CNk4 30	250 m	30°	11.3 m/s
CNk4 90	250 m	90°	11.3 m/s
CNk8 0	125 m	0°	11.4 m/s
CNk8 90	125 m	90°	11.4 m/s

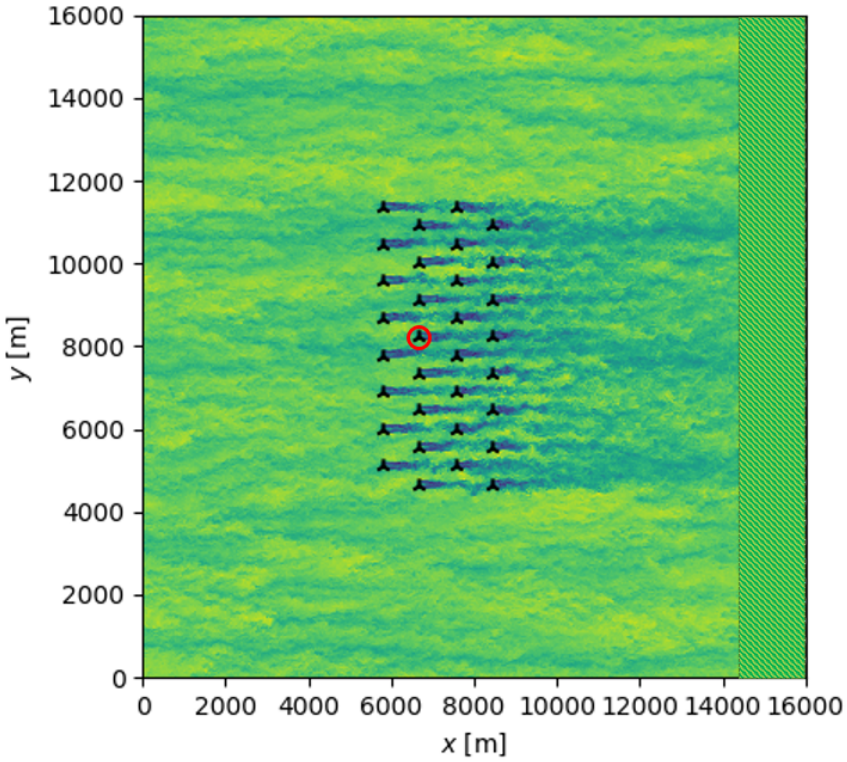

Figure 1. Planview of Reference windfarm layout in simulation domain for a PDBL inflow through a plane at hub-height. The hashed section at the end of the domain represents the fringe region. Rows are numbered 1 to 4 starting from the left row. Turbine 2.5 is circled in red.

generalized coordinates, ϕ_q and λ are the Jacobian matrix and Lagrange multipliers respectively. Q_a represents the aerodynamic loads and Q_g represents the gravitational loads. Finally, Q_v is composed of the Coriolis and gyroscopic loads.

3. Case setup

The TotalControl Reference Wind Power Plant (TC RWP) is used for all the simulations. The farm is composed of 32 DTU 10 MW turbines, with a hub height of 119 m and a rotor diameter of

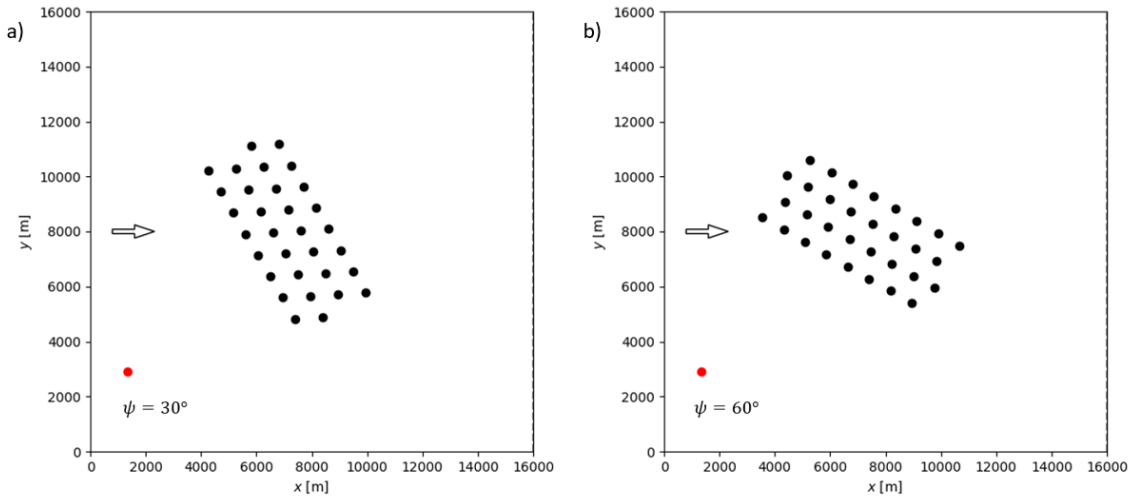

Figure 2. Reference wind farm rotated by a) 30 and b) 60 degrees to simulate different inflow wind directions

178.3 m. [8, 9] In its original form, the wind farm has a staggered arrangement of the turbines, as shown in Figure 1 . The data from the turbine highlighted in row 2 position 5 of Figure 1, from here on referred as turbine 2.5, is used for comparison of an individual turbine performance across different flow fields. Different wind inflow directions can be simulated by rotating the entire wind farm in the domain by the required wind angle, for eg. Figure 2 shows the configuration for 30° and 60° wind inflow direction. The simulation domain has a size of $16 \times 16 \times 1.5\,\mathrm{km}^3$ in the streamwise, spanwise, and vertical directions respectively. Grid resolutions are chosen at relatively standard values of $13.33 \times 13.33 \times 6.66\,\mathrm{m}^3$, resulting in a computational grid of $1200 \times 1200 \times 225 = 324 \times 10^6$ gridpoints.

The CNBL simulations are designed based on similar precursor cases for wind-farm LES discussed in Allaerts and Meyers [10]. Three different capping inversion strengths of $\Delta\theta = 2$K, 4K and 8K are considered with estimated boundary layer heights of 500 m, 250 m and 125 m respectively. Cases are forced with a constant geostrophic wind speed of $G = 12$ m/s and the base wall roughness length is $z_0 = 2 \times 10^{-4}$ m. The potential temperature lapse rate in the stably-stratified free atmosphere is $\gamma = 1$ K/km, and the temperature of the mixed layer is $\theta_m = 15°$, which is also taken as the reference temperature. The Coriolis parameter is $f_c = 10^{-4}$ s^{-1}, corresponding to a latitude of 43.43°. A PDBL simulation is also used for comparison against the CNBL simulations, with a friction velocity of $u_\star = 0.28$ m/s. The parameters of all the simulation cases are detailed in the table 1, along with the mean velocity of the precursor domain at hub height.

Wind-farm simulations are performed in a sequence of steps. First, a fully-developed turbulent boundary layer is generated in a so-called spinup simulation with periodic boundary conditions but without turbines. The precursor simulation is run for 20 hours, which allows the flow to reach a statistically stationary state. The data from the precursor simulations are then fed as inflow conditions to a set of wind-farm configurations using the concurrent precursor method. The flow is allowed to pass through the wind farm for 15 minutes to account for start-up transients, after which data collection and computation of flow statistics is done. The windfarm simulations are run for a time period of 60 minutes, with a LES time step of $\Delta t = 0.5$ second. The multi-body structural solver runs at a much faster rate with a time step of $\Delta t_s = 0.01$ seconds.

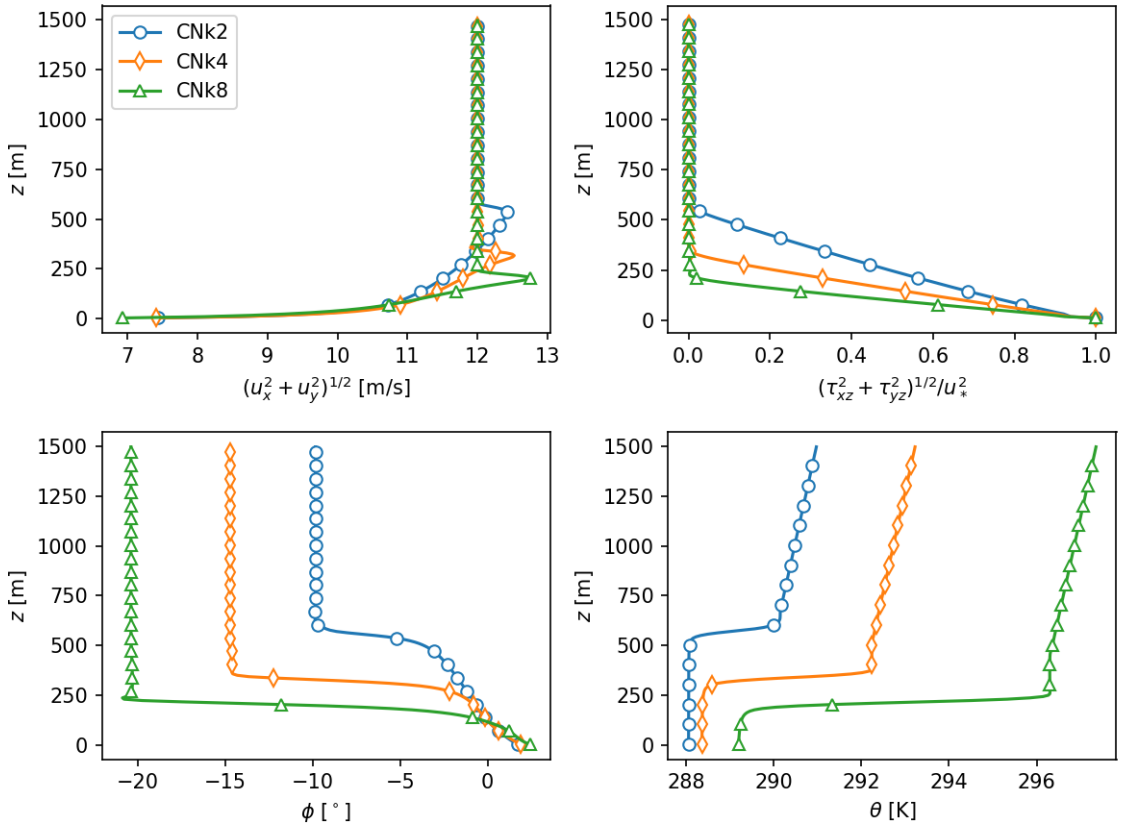

Figure 3. Flow profiles for CNBL cases with varying boundary layer heights. Top left: Horizontal Velocity. Top right: Total (Resolved + Subgrid) shear stress. Bottom left : Wind veer. Bottom right : Potential temperature

4. Results

The initial conditions for the mean wind velocity vector along the domain height as well as the temperature are shown for the CNk2 ,CNk4 and CNk8 cases in Figure 3. Smooth transition can be observed between the velocities and temperatures in the boundary layer below the capping inversion (characterized by veered and sheared velocities with well-mixed temperature) and also in the free atmosphere above it (with uniform velocities and stable free-atmosphere stratification). The average row power is presented in Figure 4 a). A power spike can be observed in row 3 of the 30° farm configuration as the top most turbine in this row is operating in un-waked conditions (evident in Figure 2a), therefore boosting average row power. The 60° wind inflow case has highest average row power in rows 3 and 4 (with row number convention taken from the staggered configuration of Figure 1), due to 2 and 1 turbines operating in un-waked conditions at the top of each row respectively. Conversely, the 90° cases have the lowest row average power due to aligned configuration. As a result, the CNk2 60 case has the highest farm power output of all the simulated cases (Figure 4 b).

From Figure 3, the velocity across the rotor plane in the CNk8 case can be seen to be consistently higher than that in the CNk4 case, hence it would be expected to obtain a higher wind farm power production in CNk8 90 than in CNk4 90. However, this is not the case as the power output of CNk4 90 is found to be marginally higher, as shown in Figure 4 b). To investigate this discrepancy, a wake deficit analysis was conducted to study the effect of the

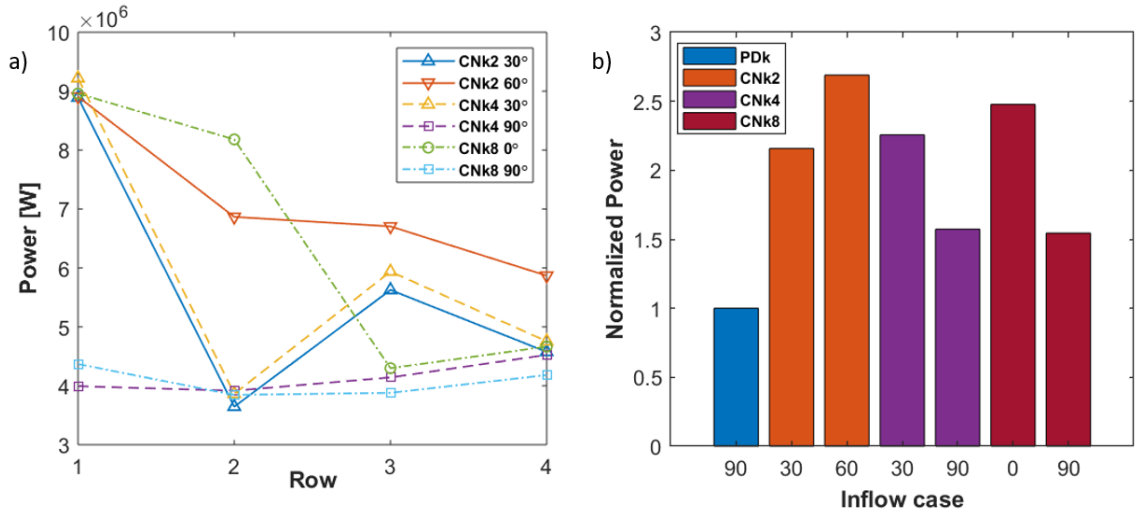

Figure 4. Average row power for different CNBL inflow cases. Rows are numbered left to right in the staggered representation of Figure 1 b) Total wind farm power output, normalized by PDk 90 case

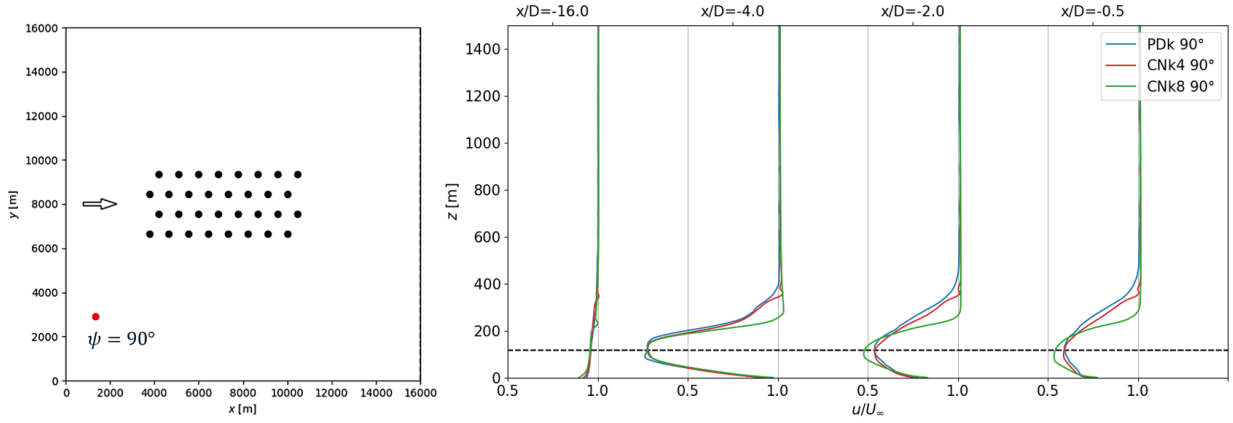

Figure 5. a) Fully aligned farm configuration for 90° inflow direction cases, b) Time averaged wake deficit at inflow planes upstream of turbine 2.5, normalized by mean inflow velocity at a point far upstream from the windfarm. Horizontal dashed line signifies hub height (119 m)

inflow cases on wake mixing and recovery. Figure 5 b) shows the vertical velocity deficit profiles at planes upstream of the turbine 2.5 for the fully aligned windfarm configuration shown in Figure 5 a), for the cases PDk 90, CNk4 90 and CNk8 90. It can be seen that while the wake deficit magnitudes at a plane 4D upstream of the turbine is similar for the 3 cases, the wake recovery of CNk4 is better than CNk8. This leads to a higher inflow velocity available at a plane 1D upstream of the turbine 2.5 across the rotor plane, resulting in larger power production. These results are in line with the observations made by Allaerts and Meyers in their study on the effect of capping inversion strength on wind farm performance. The stronger capping inversion strength of CNk8 limits the amount of energy that can be entrained into the farm from the air above it, reducing power production [11].

The effect of capping inversion strength and boundary layer height on wake mixing can be further studied in Figure 6, where the instantaneous axial velocity profile is plotted in the

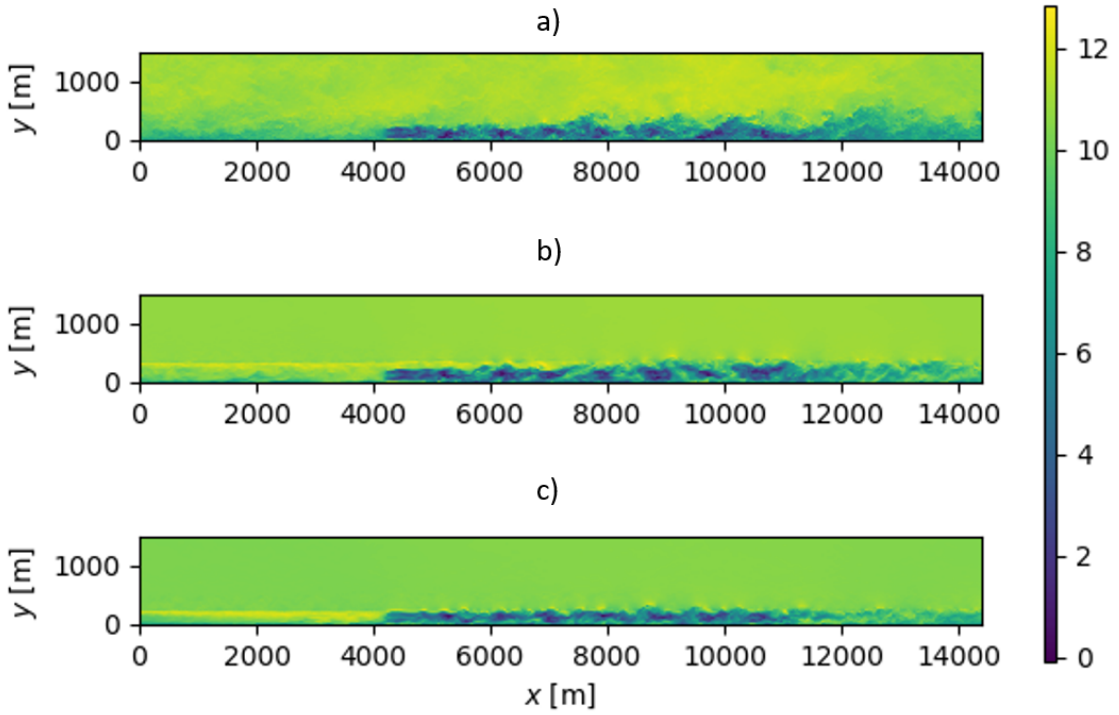

Figure 6. Instantaneous horizontal flow field in m/s at a cross section of the wind farm showing eight DTU 10MW turbines for a) PDk 90 b) CNk4 90 c) CNk8 90

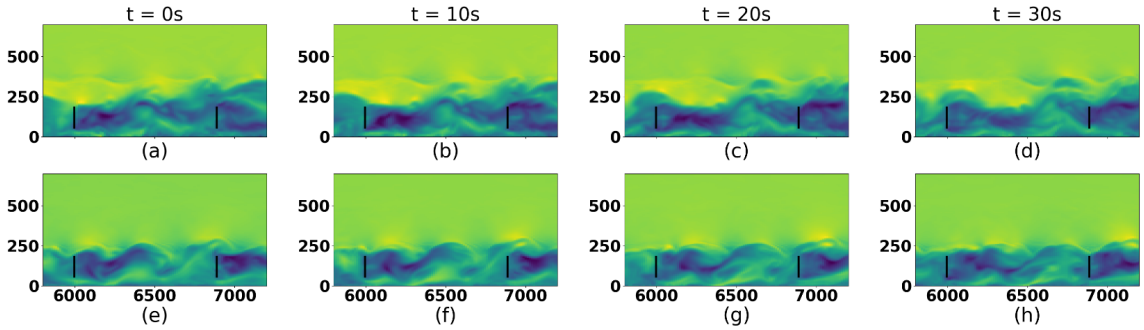

Figure 7. Inflow axial velocity time series for the turbine 2.5 operating in the wake of an upstream turbine. Figures (a)-(d) correspond the CNk4 90 case and Figures (e)-(h) correspond to CNk8 90 case over a 30 second interval

streamwise direction for the fully aligned PDk 90, CNk4 90 and CNk8 90 cases. In the lowest boundary layer of 125 m of CNk8, the flow can be seen to be more chaotic than the other cases, with perturbations originating at the inversion layer due to the presence of the windfarm, and propagating downstream. While these perturbations exist in the inversion layer of CNk4 as well, their strength and effect on the turbine wakes in CNk8 is more pronounced due to the close proximity of the wind turbine to the capping inversion. Observing a time series of the inflow velocity field of turbine 2.5 (Figure 7), the effect of these perturbations can be seen in the wakes of the upstream turbine in the form of oscillatory wake structures.

Comparing the time history of out of plane blade root bending moments in the turbine 2.5 (Figure 8) , highest moments can be observed in the CNk8 0 case as the turbine is operating in

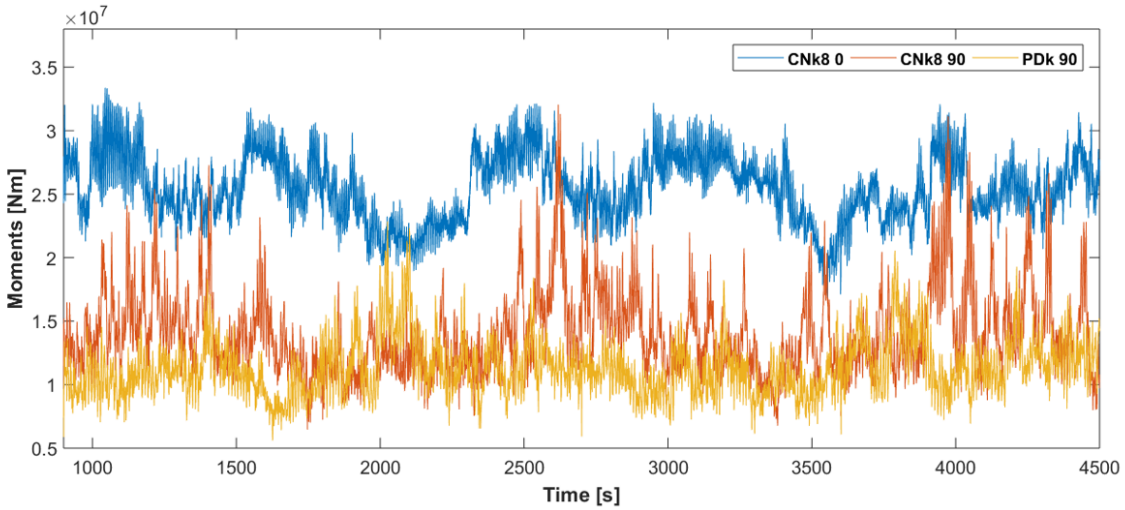

Figure 8. Out of plane blade root bending moments of the turbine 2.5

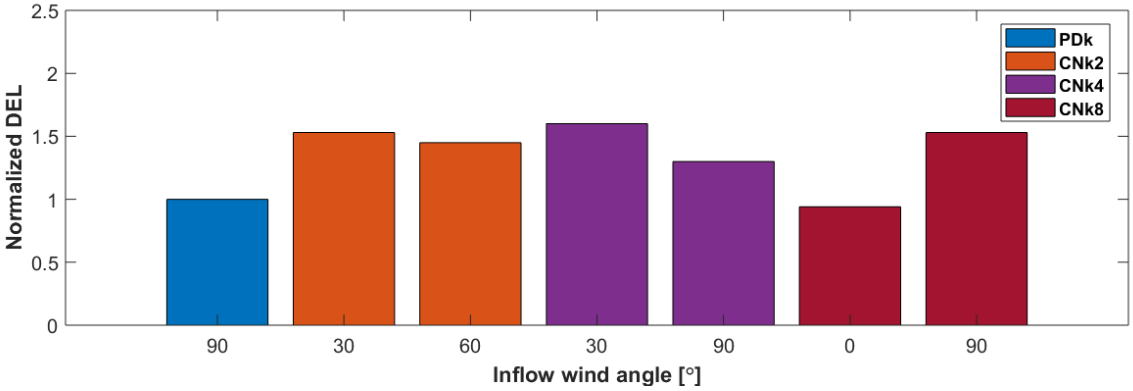

Figure 9. Out of plane blade root bending moment DEL for turbine 2.5, normalized by PDk 90 case

an unwaked condition. The PDk 90 and CNk8 90 cases have moments of lower magnitude due to the turbine operating in a waked condition in the fully aligned configuration. However, the larger variation in moments results in greater structural fatigue.

To determine the effect of fatigue, we use the damage equivalent loads (DELs) to compare the load histories of the same turbine across different cases. DEL is computed using the Palmgren-Miner rule and the Wohler equation to account for accumulating fatigue damage caused to the wind turbine components by the fluctuating structural loads [12]. The loads time series are counted and binned into individual cycles using the rainflow-counting algorithm , and for the wind turbine blades the components follow the Wohler's curve with a slope coefficient equal to 10 [13, 14]. The results of the DEL analysis for out of plane blade root bending moments for turbine 2.5 have been plotted in Figure 9, and as expected, DEL for the cases in which turbine 2.5 is operating in waked conditions is significantly higher than the ones in which the turbine is facing un-waked free stream velocity. Amongst the fully aligned cases, the DEL for the CNk8 90 case is greatest. This can be attributed to the larger variation in the inflow velocity field in the CNk8 90 case due to the oscillatory structures in the inflow flow field, as observed in Figure 7.

5. Conclusions

The purpose of the given study was to study the effect of conventionally neutral boundary layer height on wind farm performance. To this effect, wind farm power output, turbine structural fatigue and wake mixing in the farm were investigated. A series of LES simulations comprising of inflows of 3 different conventionally neutral boundary layer heights, $500\,m, 250\,m$ and $125\,m$, across staggered and aligned wind farms were performed. A pressure driven boundary layer of $1500\,m$ height was also simulated for comparison. It was observed that oscillatory structures developed in the shallowest boundary layer (CNk8 cases) which were not present in the cases with higher boundary layers. The reason for the generation of these structures could be attributed to the close proximity of the turbine to the capping inversion. These structures have a negative impact on turbine performance, leading to lower energy extraction and greater structural fatigue in downstream turbines.

Some remarks must be made regarding the current study. Due to the computationally expensive nature of the simulations, covering every possible combination of boundary layer height and wind farm orientation was not possible. Further studies can be performed to cover the missed cases and perform a more comprehensive analysis. Additionally, while conventionally neutral boundary layers of varying heights occur often in offshore conditions, the CNk8 case with 125m boundary layer height is an extreme case which was studied to understand the effect of a turbine operating at the edge of a boundary layer. Such low conventionally neutral boundary layer heights may not occur in reality, but the study is still useful to understand the performance of future turbines of larger rotor diameters operating at the edge of, or across a capping inversion. An energy tube analysis as performed by Allaerts and Meyers can also be a topic of future work to further study how these oscillatory structures affect boundary layer growth and energy extraction by the farm [15].

Acknowledgments

The authors have received funding from the European Unions Horizon 2020 programme (TotalControl, grant no. 727680). The computational resources and services used in this work were provided by the VSC (Flemish Supercomputer Center), funded by the Research Foundation Flanders (FWO) and the Flemish Government department EWI.

References

[1] Calaf M, Meneveau C and Meyers J 2010 *Physics of Fluids* **22** 015110
[2] Porté-Agel F, Wu Y T, Lu H and Conzemius R J 2011 *Journal of Wind Engineering and Industrial Aerodynamics* **99** 154 – 168 ISSN 0167-6105
[3] Allaerts D and Meyers J 2015 *Physics of Fluids* **27** 065108
[4] Goit J and Meyers J 2015 *Journal of Fluid Mechanics* **768** 5–50
[5] Stevens R J, Graham J and Meneveau C 2014 *Renewable Energy* **68** 46 – 50 ISSN 0960-1481
[6] Munters W, Meneveau C and Meyers J 2016 *Boundary-Layer Meteorology* **159**
[7] Vitsas A and Meyers J 2016 *Journal of Physics Conference Series* **753** 082020
[8] Bak C, Zahle F, Bitsche R, Kim T, Yde A, Henriksen L, Hansen M, Blasques J, Gaunaa M and Natarajan A 2013 The dtu 10-mw reference wind turbine
[9] Andersen S, Madariaga A, Merz K, Meyers J, Munters W and Rodriguez C 2018 Reference wind power plant d1. 03
[10] Allaerts D and Meyers J 2017 *Journal of Fluid Mechanics* **814** 95–130
[11] Allaerts D and Meyers J 2014 *Journal of Physics: Conference Series* **524** 012114
[12] Sutherland H 1999 Fatigue analysis of wind turbines
[13] Freebury G and Musial W 2000 *ASME Wind Energy Symposium*
[14] Downing S and Socie D 1982 *International Journal of Fatigue* **4** 31 – 40 ISSN 0142-1123
[15] Meyers J and Meneveau C 2013 *Journal of Fluid Mechanics* **715** 335–358